

Water vapor variability in the tropics and its links to dynamics and precipitation

Igor I. Zveryaev

P. P. Shirshov Institute of Oceanology, Russian Academy of Sciences, Moscow, Russia

Richard P. Allan

Environmental Systems Science Centre, University of Reading, Reading, UK

Received 31 March 2005; revised 3 June 2005; accepted 18 July 2005; published 12 November 2005.

[1] The distribution and variability of water vapor and its links with radiative cooling and latent heating via precipitation are crucial to understanding feedbacks and processes operating within the climate system. Column-integrated water vapor (CWV) and additional variables from the European Centre for Medium-Range Weather Forecasts (ECMWF) 40-year reanalysis (ERA40) are utilized to quantify the spatial and temporal variability in tropical water vapor over the period 1979–2001. The moisture variability is partitioned between dynamical and thermodynamic influences and compared with variations in precipitation provided by the Climate Prediction Center Merged Analysis of Precipitation (CMAP) and the Global Precipitation Climatology Project (GPCP). The spatial distribution of CWV is strongly determined by thermodynamic constraints. Spatial variability in CWV is dominated by changes in the large-scale dynamics, in particular associated with the El Niño–Southern Oscillation (ENSO). Trends in CWV are also dominated by dynamics rather than thermodynamics over the period considered. However, increases in CWV associated with changes in temperature are significant over the equatorial east Pacific when analyzing interannual variability and over the north and northwest Pacific when analyzing trends. Significant positive trends in CWV tend to predominate over the oceans while negative trends in CWV are found over equatorial Africa and Brazil. Links between changes in CWV and vertical motion fields are identified over these regions and also the equatorial Atlantic. However, trends in precipitation are generally incoherent and show little association with the CWV trends. This may in part reflect the inadequacies of the precipitation data sets and reanalysis products when analyzing decadal variability. Though the dynamic component of CWV is a major factor in determining precipitation variability in the tropics, in some regions/seasons the thermodynamic component cancels its effect on precipitation variability.

Citation: Zveryaev, I. I., and R. P. Allan (2005), Water vapor variability in the tropics and its links to dynamics and precipitation, *J. Geophys. Res.*, 110, D21112, doi:10.1029/2005JD006033.

1. Introduction

[2] The distribution of water vapor and its condensation as cloud is crucial in determining radiative cooling and latent heating of the atmospheric column. The atmospheric temperature profile in turn influences the maximum concentration of water vapor that the atmosphere can hold before condensation takes place. Including the interaction with the large-scale dynamics of the atmosphere, the possibilities for feedback loops involving cloud, water vapor and temperature are considerable.

[3] It is only possible to represent the numerous feedbacks involving water vapor by developing comprehensive global climate models that encapsulate the entire hydrological cycle. Using such models to conduct climate prediction

experiments results in a large spread in the climate sensitivity to a particular radiative forcing such as carbon dioxide doubling [e.g., *Intergovernmental Panel on Climate Change (IPCC)*, 2001]. This uncertainty stems primarily from differences in hydrological feedback processes, in particular involving cloud processes.

[4] While it is conceptually useful to consider feedbacks due to cloud, water vapor or temperature lapse rate in isolation, the mechanisms from which feedback loops occur usually involve many such variables. For example, it is important to understand feedbacks involving water vapor and other parameters such as precipitation [e.g., Bretherton *et al.*, 2004; Trenberth *et al.*, 2003], evaporation and dynamical transport [e.g., Gershunov and Roca, 2004; Sohn *et al.*, 2004], convection and the conversion of cirrus outflow to vapor [e.g., Soden, 2004; Luo and Rossow, 2004] and dynamical feedbacks involving subtropical dry zones [e.g., Sohn and Schmetz, 2004].

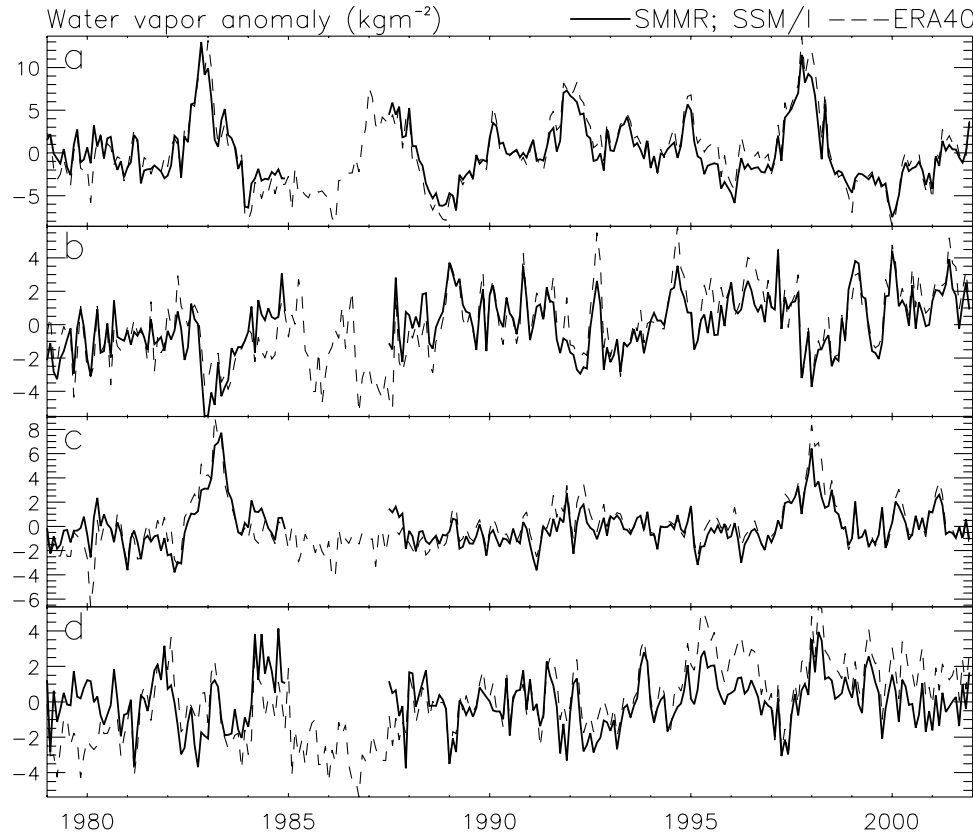


Figure 1. Anomaly time series of CWV (kg m^{-2}) for ERA40, SMMR (1979–1984), and SSM/I (1987–2001) for ocean-only area-weighted monthly averages: (a) tropical central Pacific (180° – 220° E, 10° S to 10° N), (b) northern subtropical central Pacific (160° – 200° E, 10° – 30° N), (c) subtropical southeastern Pacific (250° – 290° E, 5° – 25° S), and (d) equatorial Atlantic (0° – 40° W, 10° S to 10° N).

[5] In the present study we use water vapor and dynamical products from the European Centre for Medium-Range Weather Forecasts (ECMWF) 40-year reanalysis (ERA40) in combination with precipitation observations to quantify the present-day variability of low-latitude water vapor and its links with dynamics and precipitation. Documenting the relationship between such variables is crucial in understanding the climate feedback processes involving water vapor.

[6] The paper is organized as follows. Description of the data used and analysis methods is presented in section 2. Characteristics of column-integrated water vapor (CWV) variability in the tropics are considered in section 3. Links to precipitation variability are examined in section 4. Finally, section 5 presents conclusions.

2. Data and Methods

2.1. Statistical Methods

[7] In the present study we analyze the long-term seasonal climatologies and variability of CWV and precipitation. To examine spatial-temporal structure of the long-term variations of seasonal mean CWV, we applied empirical orthogonal function (hereafter EOF) analysis based on the covariance matrix [Wilks, 1995; von Storch and Navarra, 1995]. Before the EOF analysis the annual cycle was removed from all grid point time series by subtracting from each seasonal value the respective season's long-term mean.

The long-term stationarity of the time series is preserved for the calculation of EOF through detrending the time series with a linear least squares fit. Since the analyzed time series of the CWV are relatively short, we verified robustness of the obtained leading modes of variability by application of the EOF analysis to time series of monthly anomalies of CWV (i.e., extending time series to $23 \times 3 = 69$ samples). Only significant EOF modes that were evident in analyses of both seasonal and monthly data are considered in the study. We quantify the variability over the tropical region (30° S to 30° N) by calculating local standard deviations, linear trends and by applying the EOF analysis. Previously, Zveryaev and Chu [2003] used these methods to investigate the interannual and decadal variability in tropical water vapor from the NCEP/NCAR reanalysis. Here we utilize column water vapor and additional variables from the ERA40 reanalysis and precipitation data from the Climate Prediction Center Merged Analysis of Precipitation (CMAP) and the Global Precipitation Climatology Project (GPCP). Additionally, we attempt to separate the effects of the large-scale dynamics on the water vapor fields using dynamical products from ERA40.

2.2. ERA40 Reanalysis

[8] Reanalyses of historical data are produced in much the same way as in numerical weather prediction (NWP); a general circulation model is adjusted through data assimila-

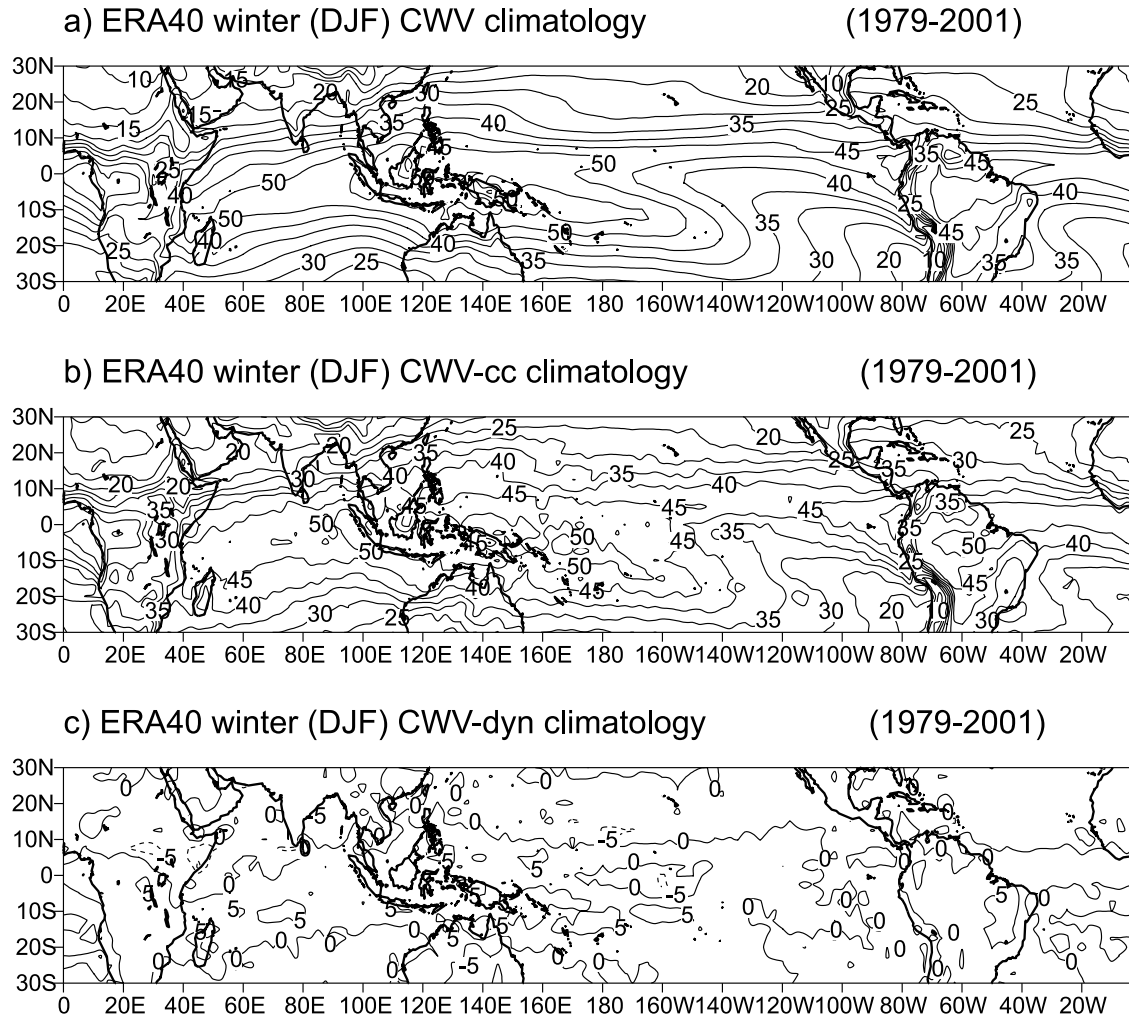


Figure 2. Winter (DJF) seasonal mean climatology of (a) column-integrated water vapor CWV and its (b) thermodynamic component CWV_{cc} and (c) dynamic component CWV_{dyn} in kg m^{-2} for ERA40 data over the period 1979–2001.

lation to optimize the agreement with both conventional and satellite observations. The resulting analysis, which provides initial conditions for operational forecast models, is useful also as a record of atmospheric conditions available globally on a model grid. The ECMWF conducted a comprehensive reanalysis (ERA40) over the period 1957–2002 using the fixed operational integrated forecast system cycle 23r4, applying three-dimensional variational assimilation. For further details and initial validation, see *Uppala et al.* [2005]. In the present study we employ monthly mean column-integrated water vapor (CWV), 1.5 m temperature ($T_{1.5\text{m}}$) and 500 hPa vertical motion fields (ω_{500}) from ERA40 on a 2.5×2.5 degree spatial grid over the period 1979–2001.

[9] Initial validation of ERA40 has suggested that CWV is well simulated over the ocean, on the basis of comparisons with microwave satellite observations from the Scanning Multichannel Microwave Radiometer (SMMR) [Wentz and Francis, 1992] and the Special Sensor Microwave Imager (SSM/I) [Wentz, 1997] over the period 1979–1999 [*Allan et al.*, 2004; *Uppala et al.*, 2005]. We also find that

ERA40 captures the seasonal climatology and standard deviation of CWV observed by SSM/I over the period 1988–1999 (not shown). While variability of tropical-mean water vapor and precipitation is thought to be inaccurate [*Allan et al.*, 2004; *Trenberth et al.*, 2005], here we concentrate on the spatial signature of CWV variability. To improve the confidence in the regional variability, we now compare time series of CWV from ERA40 with the SMMR and SSM/I satellite data. Version 5 of the SSM/I data was used in these comparisons, which consist of a set of overlapping, intercalibrated satellites (F08, F10, F11, F13, F14, F15). To provide a continuous record, we first merged the series of individual satellite records. The first and last months of each satellite record were removed from the merging process if disagreement between an additional satellite monthly tropical mean was greater than 0.5 kg m^{-2} . This assumes that such measurements are erroneous because of incomplete monthly sampling or problems with the instrument.

[10] Figure 1 shows time series of CWV for ERA40 and the SMMR or SSM/I data for four regions (see caption of

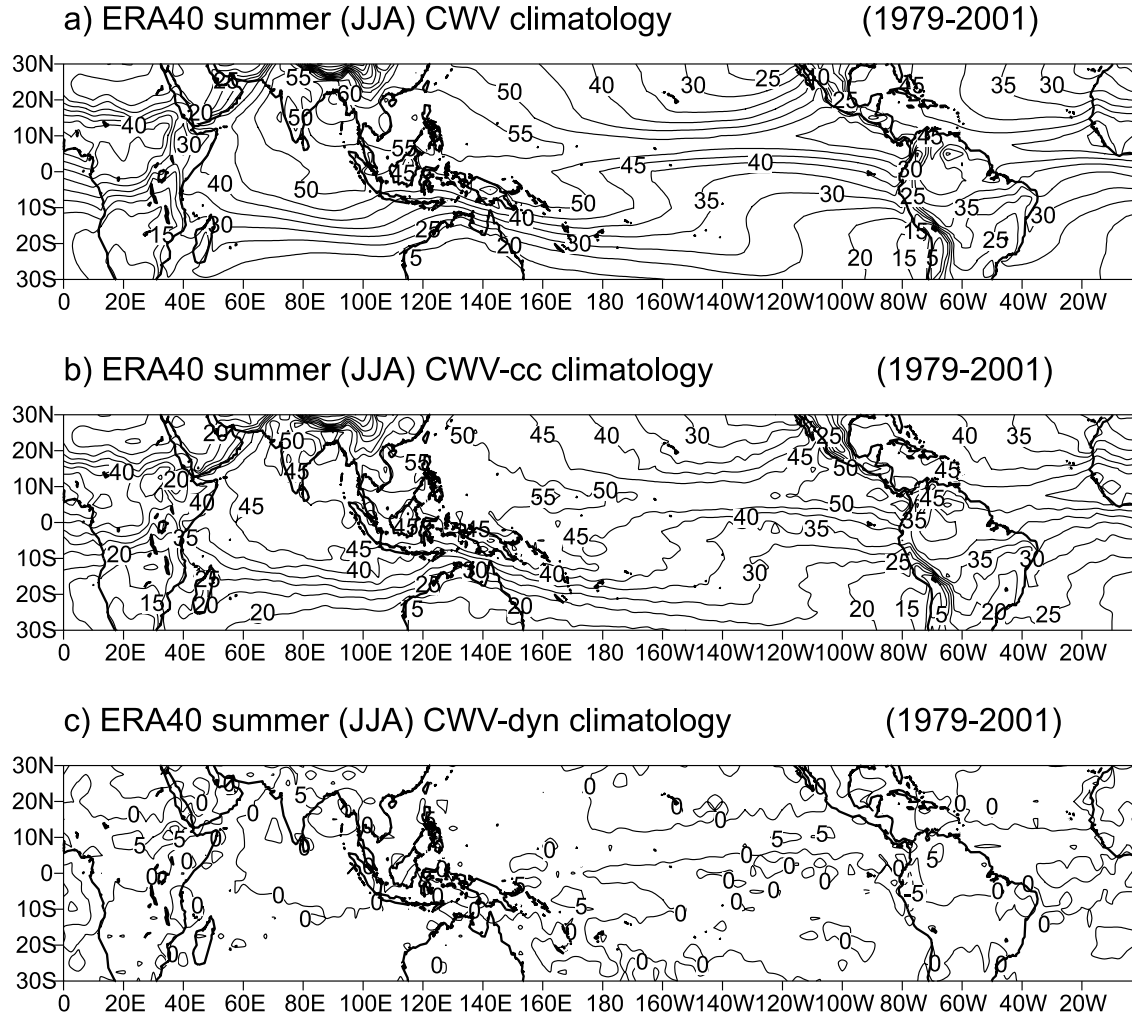


Figure 3. As Figure 2 but for summer (JJA) seasonal means.

Figure 1 for details). The mean seasonal cycle has been removed from all time series. During 1995–1996 there is evidence that ERA40 overestimates CWV for the tropical west Pacific (Figure 1a) and for the subtropical southeastern Pacific (Figure 1d). This is thought to be a result of erroneous satellite data used in the assimilation during this period [Uppala *et al.*, 2005]. Also ERA40 underestimates CWV during 1979 over the equatorial Atlantic compared with SMMR data. This highlights the need for caution in the interpretation of the ERA40 data, which suffer from errors relating to model parametrizations and data assimilation. However, Figure 1 shows that there is generally good agreement between ERA40 and the satellite data over interannual and decadal timescales to within the expected root mean squared calibration error of 1.2 kg m^{-2} for SSM/I data [Wentz, 1997].

2.3. Precipitation Data

[11] We employed monthly mean precipitation data from the CMAP data set for 1979–2001 [Xie and Arkin, 1996, 1997]. The data were obtained from five kinds of satellite estimates (GOES precipitation index (GPI), outgoing-long-wave-radiation-based precipitation index, Special Sensor

Microwave Imager (SSM/I) scattering, SSM/I emission and microwave sounder unit values). This data set consists of pentad and monthly averaged precipitation rate values (mm/d) for the time period January 1979 to December 2001. The data have a 2.5° latitude by 2.5° longitude spatial resolution and global coverage. Though these data have a relatively short time history, their advances over other products are the global coverage, including land and oceanic/marine regions, and temporal resolution, that provides an opportunity to investigate intraseasonal fluctuations of precipitation along with its interannual variations. The CMAP data are believed to be among the most reliable data on precipitation. In comparisons with surface rain gauges, Xie and Arkin [1997] found root mean squared errors for 6 years of CMAP data of about 25% when considering grid points of 5 or more gauges. The data are available online at <ftp://ftpprd.ncep.noaa.gov/pub/precip/cmap>.

[12] We also used monthly mean precipitation data from the Version 2 of the GPCP data set for 1979–2001 [Huffman *et al.*, 1997; Adler *et al.*, 2003]. Input data sets for the GPCP product include Global Precipitation Climatology Centre (GPCC) rain gauge analyses, SSM/I rain rate

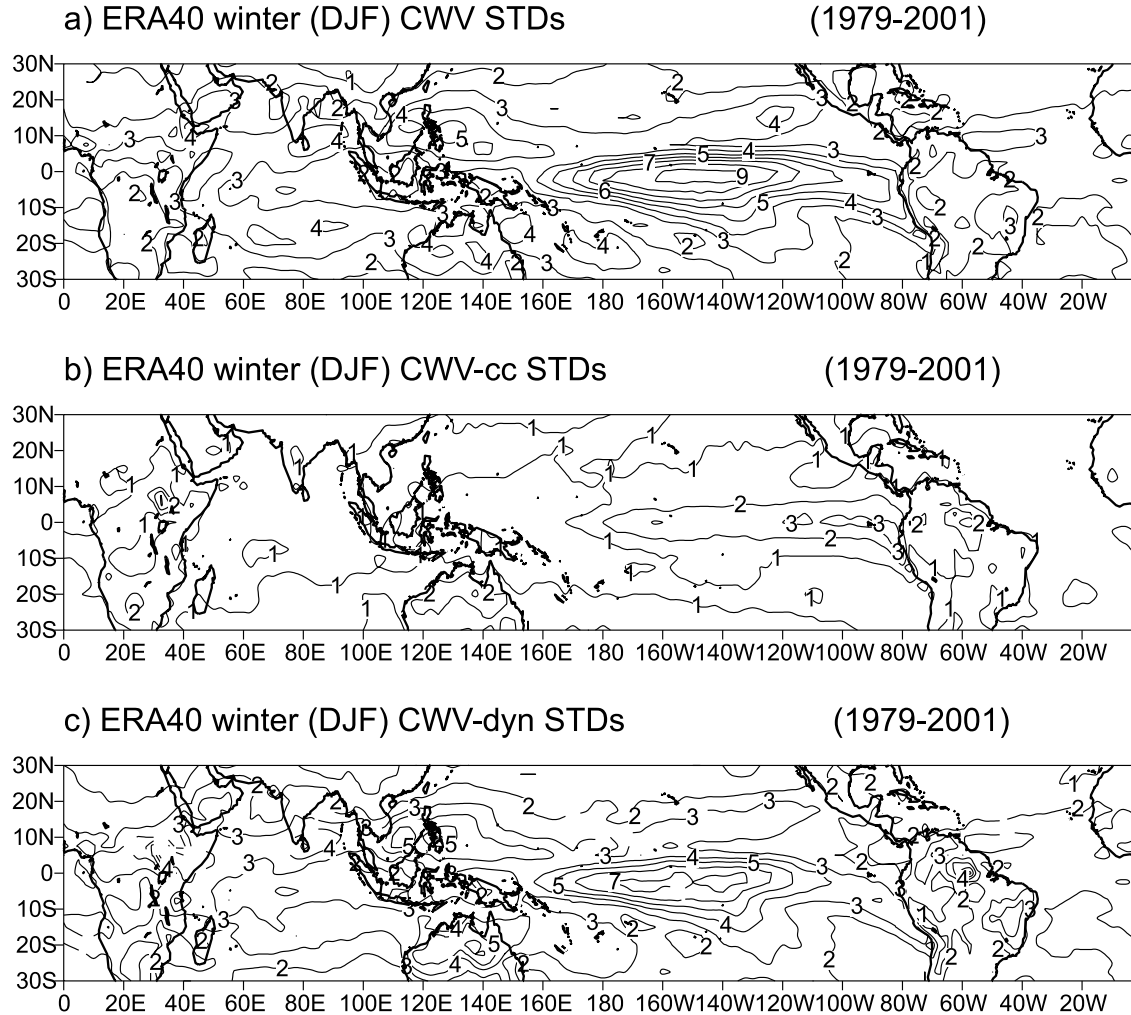


Figure 4. Standard deviations of (a) CWV and its (b) thermodynamic and (c) dynamic components in kg m^{-2} for DJF 1979–2001 means.

estimates, GPI, rain gauge data from the Global Historical Climate Network (GHCN) and Climate Assessment and Monitoring System (CAMS), TOVS-based estimates and OLR precipitation index (OPI). Adler *et al.* [2003] estimate a random and sampling error of 10–30% for GPCP data over regions of significant rainfall ($>100 \text{ mm/month}$). The GPCP monthly data set is similar in form to the CMAP, although the analysis methodologies are different. A comparison of the two products is given by Yin *et al.* [2004]. The GPCP data are available online at <http://www.ncdc.noaa.gov/oa/wmo/wdcamet-ncdc.html>.

2.4. Dynamic and Thermodynamic Contribution to Water Vapor

[13] We attempt to quantify the effects of the dynamic and thermodynamic contributions to the CWV variability by estimating the changes in moisture explained by the Clausius-Clapeyron equations. This allows us to partition the variability in water vapor between the changes in the large-scale circulation and the changes relating to thermodynamics. It has been shown previously that this type of approach is valuable in understanding cloud feedback [e.g.,

Bony *et al.*, 2004]; here we concentrate on water vapor and its links with dynamics and precipitation.

[14] To estimate the thermodynamic contribution to changes in CWV, we use only the CWV fields along with near-surface temperature and dynamical fields from ERA40. It is also possible to use satellite microwave measurements from SSM/I to estimate CWV. Here we concentrate on analyzing the ERA40 data, since the SSM/I satellite observations sample only ice-free ocean regions and do not cover entirely the period of interest, 1979–2001. To remove much of the influence of changes in large-scale circulation on CWV variations, we first use reanalysis fields to sample only grid points containing “neutral” atmospheric conditions. Neutral atmospheric conditions are defined here as

$$|\omega_{500}| < 0.015 \text{ Pa s}^{-1} \quad (1)$$

Using only the data points that met the criteria of equation (1), multiannual mean values of neutral condition CWV ($\langle \text{CWV_neutral} \rangle$) and $T_{1.5m}$ ($\langle T_{\text{neutral}} \rangle$) were calculated. The small amounts of missing data were spatially

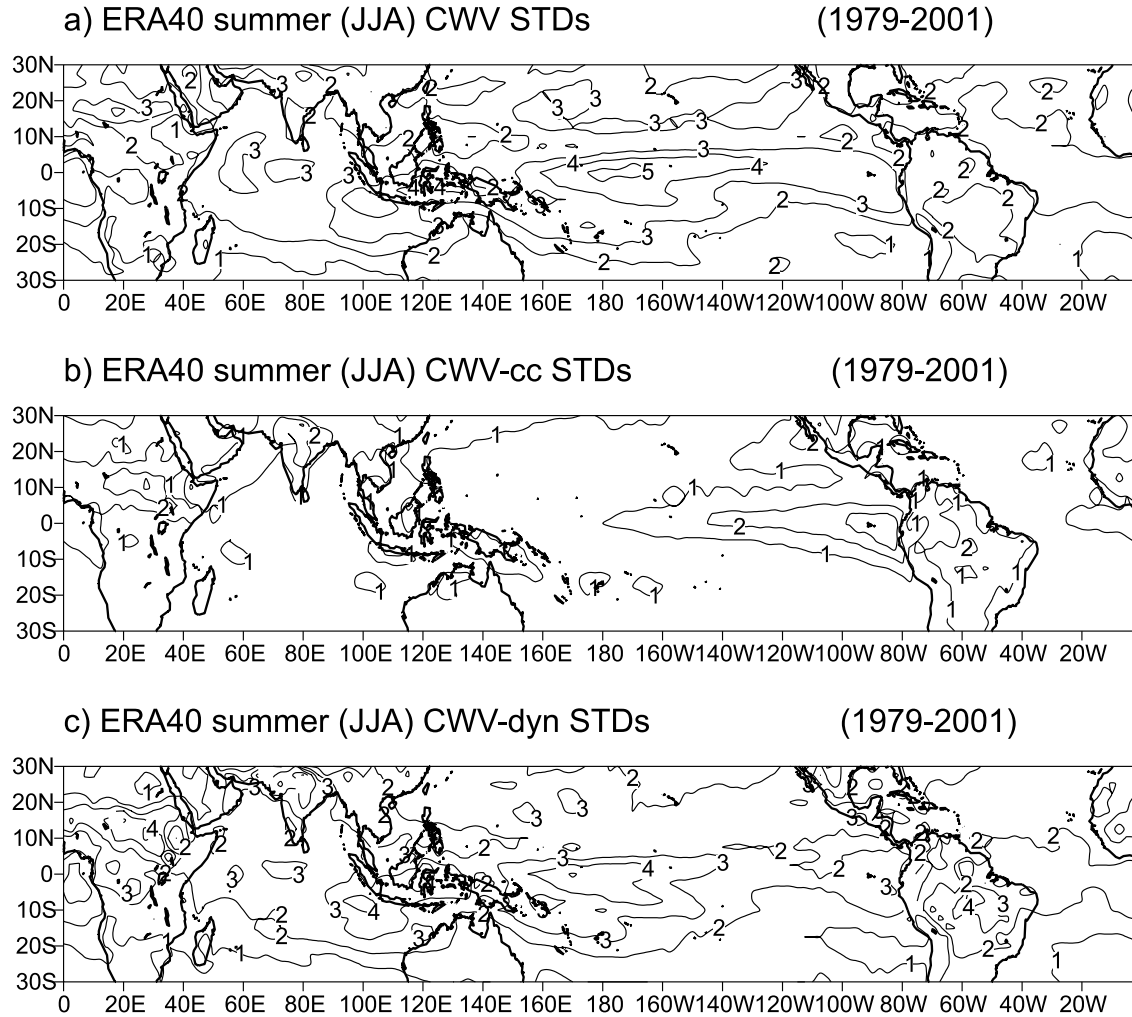


Figure 5. As Figure 4 but for JJA 1979–2001 means.

filled using bilinear interpolation. On the basis of the resulting spatial maps of $\langle \text{CWV_neutral} \rangle$ and $\langle \text{T_neutral} \rangle$, we used linear regression to derive the following thermodynamic relationship over the tropical oceans as given by Raval and Ramanathan [1989]:

$$\ln(\text{CWV_ocean}) = -14.0 + 0.059\text{T}_{1.5m}, \quad (2)$$

with correlation coefficient, $r = 0.987$, and 1-sigma uncertainty of $2 \times 10^{-4} \text{ K}^{-1}$ for the slope term. The CWV_ocean term approximates the thermodynamic relationship between CWV and T_0 in ERA40 for neutral conditions over the tropical oceans. Compared with the analysis of Raval and Ramanathan [1989], the gradient term in equation (2) (0.059 K^{-1}) is larger than that for SMMR data over the oceans (0.055 K^{-1}) and closer to the expected Clausius-Clapeyron relationship (0.069 K^{-1}). By only sampling neutral atmospheric conditions, the effects of changes in dynamics on this relationship are reduced, though not entirely removed, compared to Raval and Ramanathan [1989].

[15] The relationship in equation (2) was applied over the entire tropics, including land points, for all 276 months using monthly mean, grid point values of T_0 to calculate

CWV_ocean. CWV_ocean represents ocean conditions where boundary layer relative humidity (RH) is typically around 80%. To capture the thermodynamic changes in water vapor, an adjustment must be applied to account for spatial variations of RH that are unrelated to the large-scale dynamics. For example, land regions with little available surface water for evaporation will generally contain lower humidity than ocean regions containing similar vertical motion. The reasons for this adjustment are further outlined below.

[16] The relative humidity (RH) may be defined as the water vapor mixing ratio (q) expressed as a fraction of its theoretical saturation value (q_{sat}) determined by the Clausius-Clapeyron equation in terms of temperature T :

$$\text{RH} = q/q_{\text{sat}}(T). \quad (3)$$

It follows that for a fixed RH, the change of q with T is related to the Clausius-Clapeyron equation via $dq_{\text{sat}}(T)/dT$ multiplied by RH:

$$dq/dT = \text{RH } dq_{\text{sat}}(T)/dT. \quad (4)$$

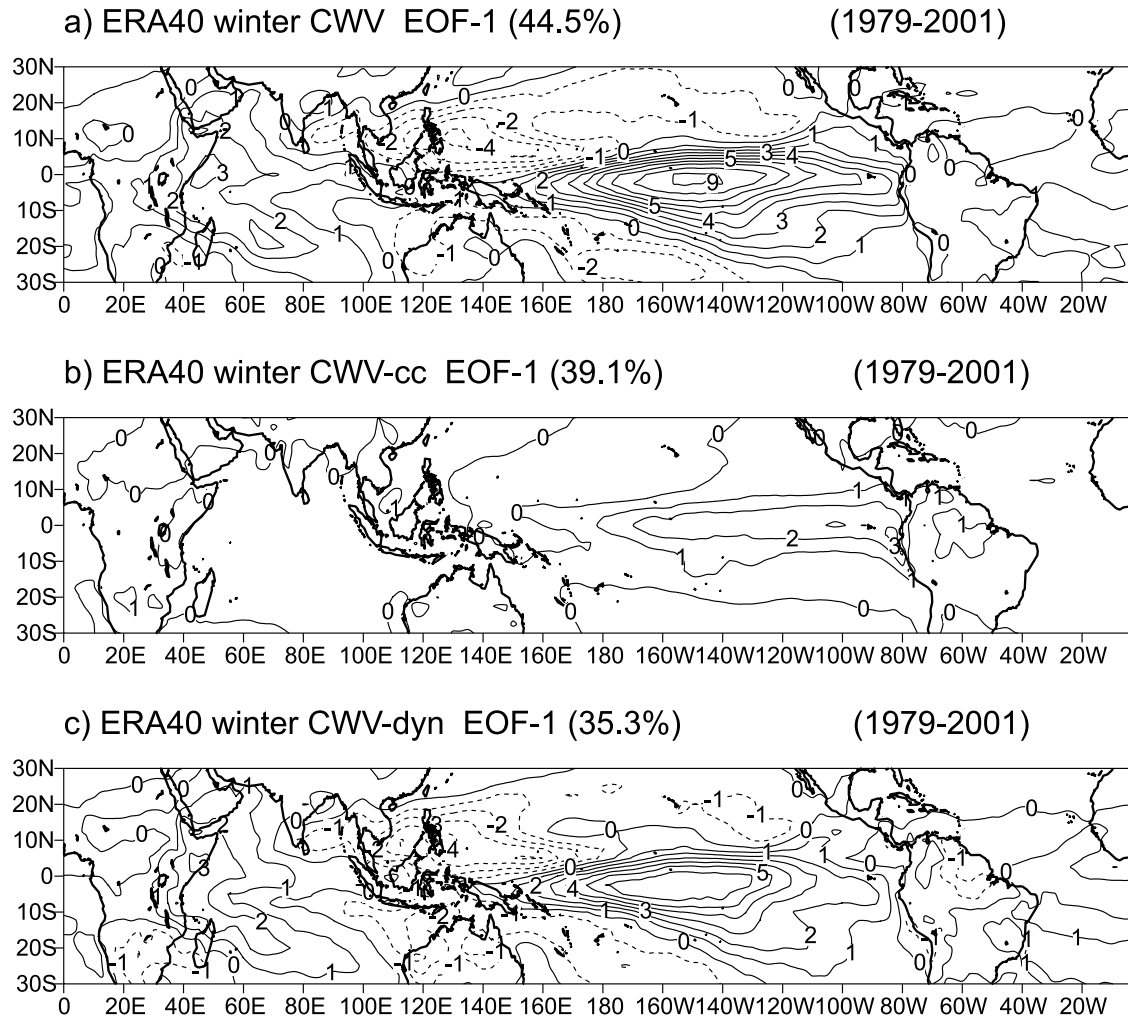


Figure 6. Spatial patterns of the first EOF modes of (a) CWV, (b) CWV_cc, and (c) CWV_dyn for DJF 1979–2001.

For low values of RH, the changes in q with T relating to the Clausius-Clapeyron equation will therefore be smaller than if RH is high.

[17] In a similar manner to Bretherton *et al.* [2004] we define an effective column relative humidity parameter, R , which here is the ratio of the multiannual monthly climatologies of CWV for (1) neutral vertical motion conditions $\langle \text{CWV}_\text{neutral} \rangle$ and (2) near-saturated oceanic conditions $\langle \text{CWV}_\text{ocean} \rangle$, calculated in equation (2):

$$R = \langle \text{CWV}_\text{neutral} \rangle / \langle \text{CWV}_\text{ocean} \rangle. \quad (5)$$

The humidity parameter, R , is independent of vertical motion and instead depends on the amount of surface water available for evaporation or horizontal advection of water vapor. Equation (5) is analogous to equation (3) with $\langle \text{CWV}_\text{neutral} \rangle$ representing q and $\langle \text{CWV}_\text{ocean} \rangle$ representing q_sat . In reality, CWV_ocean represents RH $\sim 80\%$ so it is therefore possible for R to be greater than 100%. The calculated value of R in fact ranges from about 100% over the oceans to 50% over the Sahara. It follows that the expected variation of CWV relating to the Clausius-Clapeyron relationship (CWV_cc , where the subscript

“cc” denotes Clausius-Clapeyron) is the thermodynamic relationship derived in equation (2) over the oceans (CWV_ocean) multiplied by the monthly climatology of the humidity parameter R :

$$\text{CWV}_\text{cc} = \text{CWV}_\text{ocean}(T_0) \cdot R \quad (6)$$

Finally, the dynamical component of CWV is calculated as

$$\text{CWV}_\text{dyn} = \text{CWV} - \text{CWV}_\text{cc}. \quad (7)$$

3. Variability of Column-Integrated Water Vapor

3.1. Seasonal Climatologies and Standard Deviations

[18] Figure 2 shows the seasonal mean CWV and its thermodynamic (CWV_cc) and dynamic (CWV_dyn) components for December to February (DJF) 1979–2001. The similarity between Figures 2a and 2b indicates that the CWV distribution is strongly dominated by the thermodynamic constraints. The good agreement is due to the strong influence of SST on low-altitude water vapor amount [e.g.,

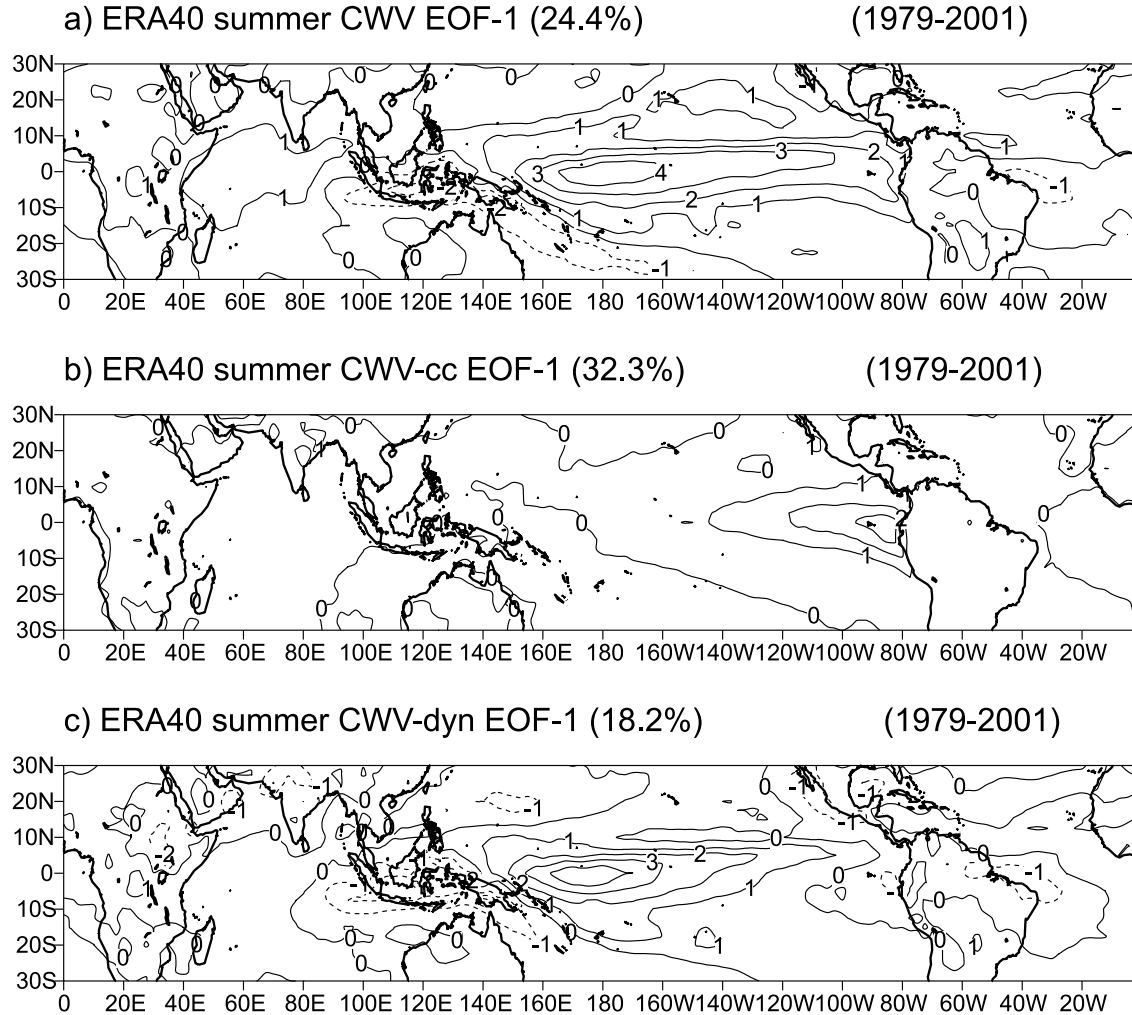


Figure 7. Spatial patterns of the first EOF modes of (a) CWV, (b) CWV_cc, and (c) CWV_dyn for JJA 1979–2001.

Raval and Ramanathan, 1989] and also in part due to the adjustment made in equation (6) that effectively accounts for the spatial variation of RH unlinked to vertical motion. Nevertheless, the subtle differences between CWV and CWV_cc indicate where the influence of dynamics on the distribution is strong. For example, CWV_cc does not capture the CWV maxima over the tropical west Pacific (TWP) and the South Pacific Convergence Zone (SPCZ). This is clearly seen by analyzing the dynamic component of CWV in Figure 2c, which shows positive values of over 5 kg m^{-2} over the TWP, the SPCZ and also over the east Pacific intertropical convergence zone (ITCZ), the Indian Ocean and also over central Africa and Brazil. Over these regions, convergence of moisture due to the large-scale dynamics augments the already high values of CWV. Over subtropical regions, CWV_dyn is generally negative. This results from the transport of low-level moisture from its source over warm subtropical oceans to the convergence zones [e.g., Gershunov and Roca, 2004].

[19] A similar picture is evident for the June to August (JJA) means in Figure 3. Major seasonal differences are detected over boreal summer monsoon regions. In particular, the largest dynamical influence occurs over the Bay of

Bengal and also over the zone connecting Ethiopia to Cameroon, relating to the Indian and African monsoon circulations. Also the east Pacific ITCZ appears more pronounced than in DJF because of both the thermodynamic and dynamic contributions to CWV. The regions of highest surface temperature also coincide with regions of ascent and convergence such that the large-scale dynamics amplify the thermodynamic maxima in CWV over these regions.

[20] The standard deviations of CWV and its components, representing their interannual variability, are displayed for DJF (Figure 4) and JJA (Figure 5). In contrast to the climatologies of CWV, CWV_dyn rather than CWV_cc dominates the local CWV variance. For example the high standard deviation of CWV in the central Pacific is primarily explained by the dynamical component, CWV_dyn. This is consistent with the variability relating to changes in the large-scale atmospheric circulation relating to the El Niño–Southern Oscillation (ENSO). The large changes in the eastern and central Pacific temperature over ENSO cycles are evident by a maximum standard deviation of about 3 kg m^{-2} in CWV_cc; in the east Pacific, the CWV_cc dominates the CWV variability. However, the much larger changes in CWV in the central Pacific relate primarily to the

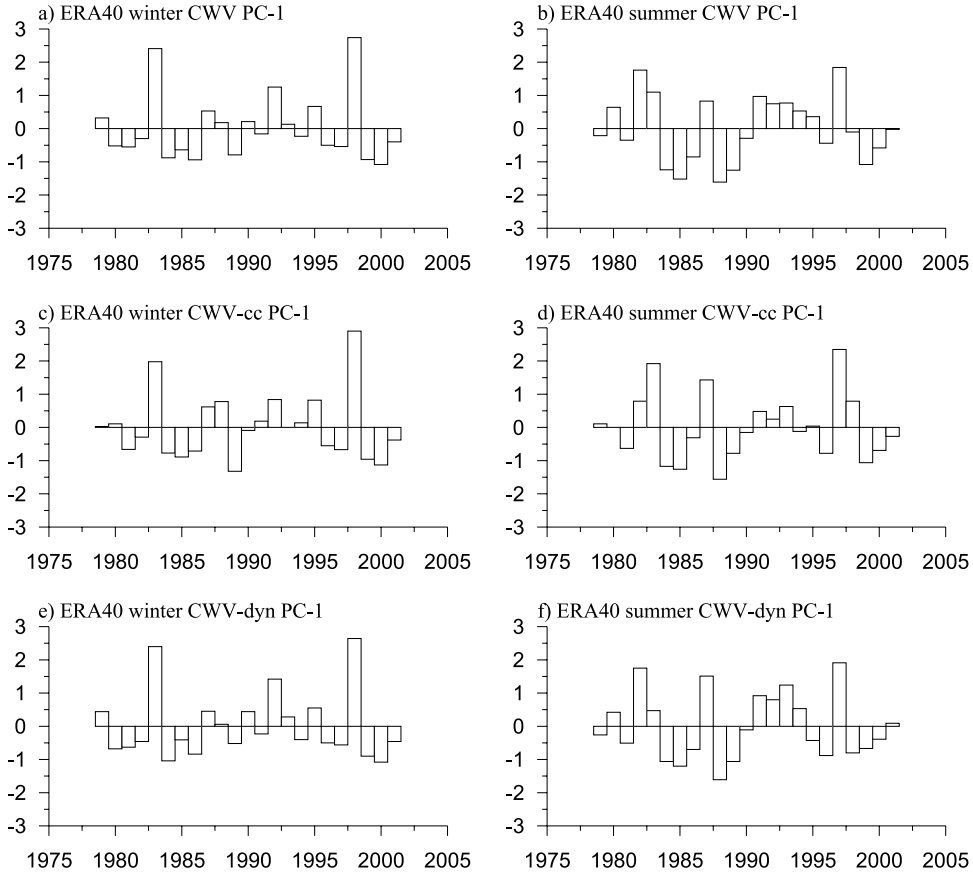


Figure 8. Principal components of the first EOF modes of (a and b) CWV, (c and d) CWV_cc, and (e and f) CWV_dyn for DJF (Figures 8a, 8c, and 8e) and JJA (Figures 8b, 8d, and 8f), 1979–2001.

movement of the convective centre from the tropical west Pacific to the central Pacific.

[21] For JJA, the dynamical changes in CWV also dominate the interannual variability away from the eastern equatorial Pacific where both dynamic and thermodynamic changes in CWV are important. The variation in CWV_dyn and CWV_cc in the central Pacific are much smaller in magnitude and spatial extent in JJA than DJF. This may relate to the phase locking of ENSO with the seasonal cycle [e.g., Spencer, 2004] with the mature phase of ENSO tending to coincide with boreal winter.

[22] Comparing Figure 2 to Figure 5, it is interesting to note that over the central equatorial Pacific around 160°W , where moisture variability is large, the climatological CWV is lower than that predicted by CWV_cc. This suggests that the local circulation acts to reduce moisture for this region, most especially in DJF. During El Niño, this region becomes a moisture sink while usually moisture is transported away from this area. A similar but smaller magnitude effect is also apparent off the coast of eastern Africa (negative CWV_dyn).

3.2. Leading EOF Modes

[23] We now quantify the spatiotemporal signature of CWV variability by computing EOFs for DJF (Figure 6) and JJA (Figure 7). The first EOF of CWV for DJF (Figure 6a) explains 44.5% of the total variance. The magnitude exhibits strong similarities to the standard devi-

ation shown in Figure 4a. The maxima over the tropical central and eastern Pacific and over the western Indian Ocean are of opposite sign to the signal over the tropical western Pacific and subtropical Pacific. The spatial signature of CWV variability is linked to ENSO; the principle component shown in Figure 8a is strongly positive for the 1982/3 and 1997/8 El Niño events.

[24] The EOF signature for CWV and CWV_dyn show a marked similarity (Figures 6a and 6c), as do the corresponding principle components (Figures 8a and 8c), suggesting that the spatial signature of CWV variability is explained primarily by the dynamic component. This is consistent with this mode of variability being linked to ENSO in which there is a large reorganization of the atmospheric circulation characterized, in particular, by significant longitudinal displacement of the Walker circulation cell. However, the thermodynamic contribution to CWV variations (Figure 6b) is significant over the equatorial central and eastern Pacific because of the large changes in SST. Over these regions the large CWV variability explained by changes in atmospheric circulation are compounded by the Clausius-Clapeyron relationship between saturated vapor pressure and temperature. The CWV_cc principal component in Figure 8 shows subtle differences to CWV and CWV_dyn, with a stronger signal from the evolution through a complete ENSO cycle from 1986 to 1989 and a weaker signal from the 1992 El Niño. EOF-1 patterns and principal components show strong similarity to

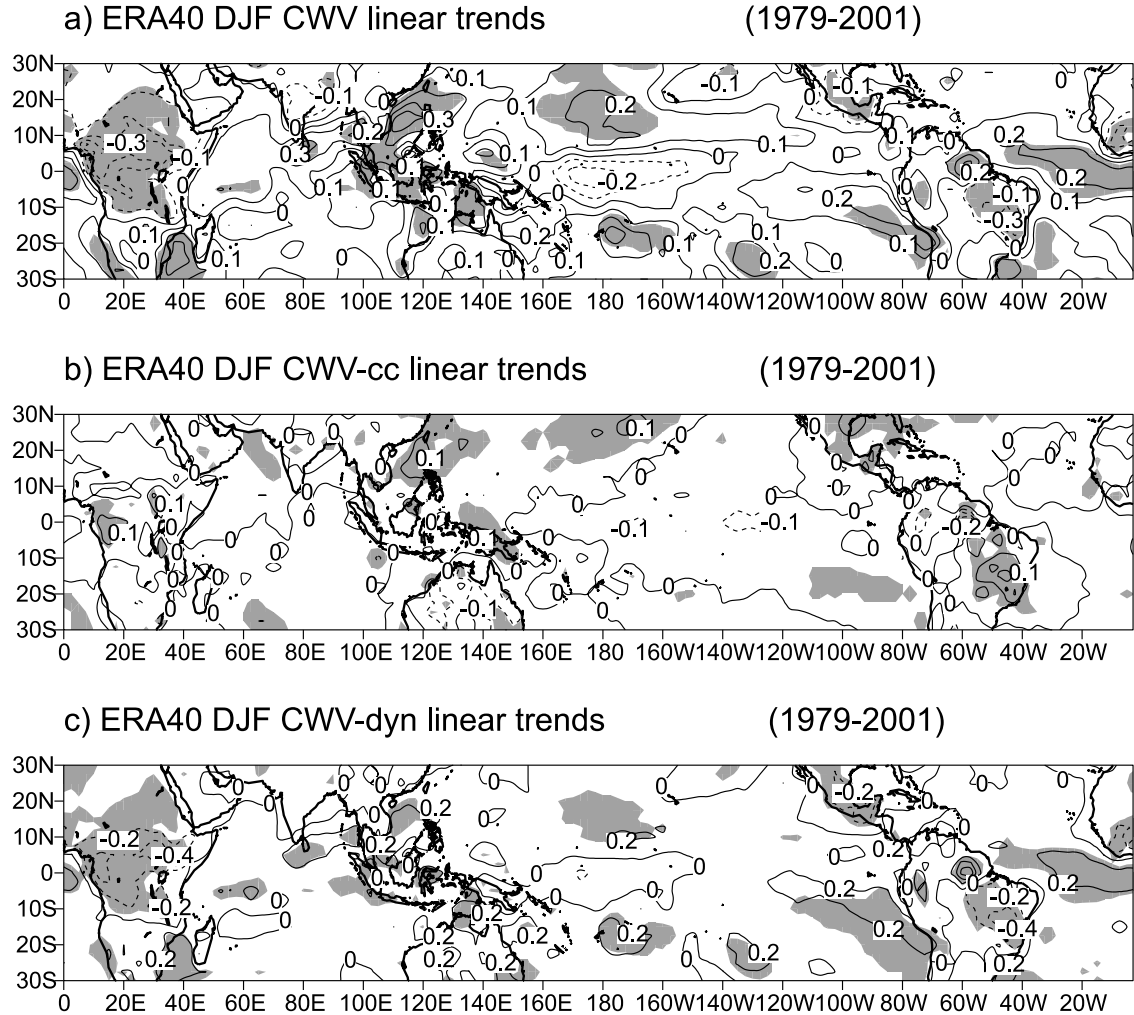


Figure 9. Linear trends for (a) CWV, (b) CWV_cc, and (c) CWV_dyn in kg m^{-2} for DJF, 1979–2001. Dashed curves depict negative trends, and shaded areas indicate 95% significance level.

the combined GPCP-CMAP precipitation EOF calculated over a similar period but for monthly means [Yin *et al.*, 2004]. This highlights the strong positive correlation between CWV and precipitation over the Pacific relating to the large changes in atmospheric circulation that occur during ENSO evolution.

[25] The first EOF of CWV for JJA (Figure 7a) shows similarity to the corresponding signal for DJF. However, the magnitude of the signal over the Pacific is smaller, being confined to the equatorial belt. The local maximum in signal over this region is further west for JJA (180°W) than DJF (150°W). This relates to the more mature phase of El Niño preferentially coinciding with DJF [e.g., Diaz *et al.*, 2001]. The first EOF mode of the dynamic component of CWV is not well separated statistically from other modes according to the test of North *et al.* [1982]. Nevertheless, the maximum magnitudes of the first EOF mode for CWV_dyn correspond with the maxima in CWV standard deviation in Figure 5 suggesting that this mode of variability is robust. Similar to DJF, the variability in CWV is dominated by the dynamic component (Figure 7c) apart from over the eastern equatorial Pacific where the thermodynamic signal is significant (Figure 7b). The principal component time

series show similarity between CWV_dyn and CWV for JJA. Consistent with DJF, CWV_cc displays a weaker 1992 El Niño signal and a stronger 1987 El Niño signal. This suggests that the SST changes amplified the CWV variability during the 1986/7 El Niño but did not strongly influence the 1992 El Niño.

4. Links Between Column-Integrated Water Vapor and Precipitation

4.1. Linear Trends

[26] In the previous section, we found large interannual variation in CWV that is dominated by changes in the large-scale dynamics associated with ENSO variability. Of additional interest is the slowly evolving changes or trends in water vapor. This is of particular interest to climate change where increasing atmospheric water vapor amounts are expected to accompany global warming [IPCC, 2001]. It is an important question as to whether the trends over the period 1979–2001 are associated with this thermodynamic constraint or rather with decadal changes in the large-scale dynamical fields.

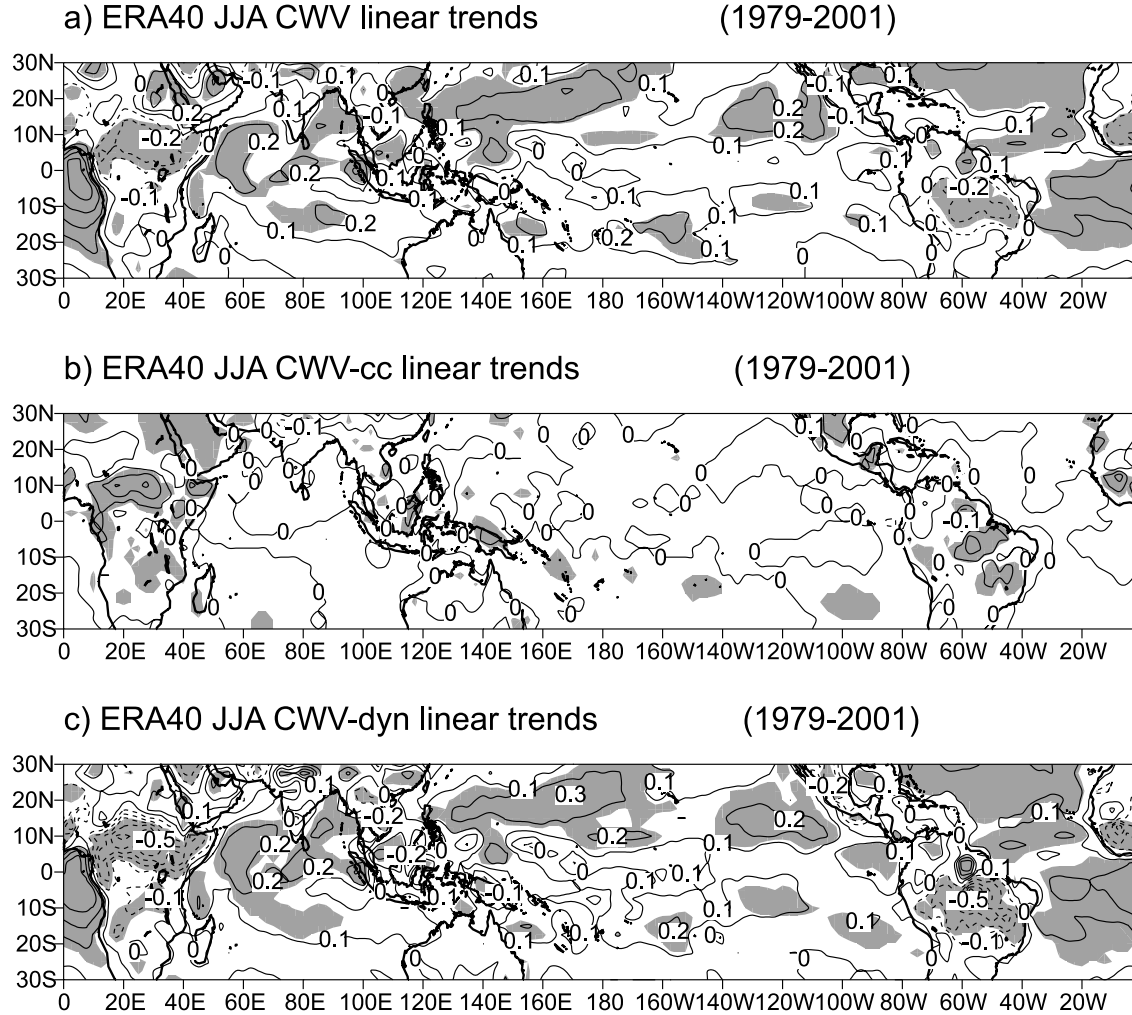


Figure 10. As Figure 9 but for JJA, 1979–2001.

[27] We show the linear trends in CWV, CWV_cc and CWV_dyn for DJF (Figure 9) and JJA (Figure 10). Solid contours denote positive trends and dashed contours highlight negative trends. Trends significant at the 95% confidence level according to Student's *t*-test [Bendat and Piersol, 1966] are shaded. In this section all trends' values are present per year.

[28] Significant trends over the ocean are primarily positive; for example, the north central Pacific at 180°E, the equatorial Atlantic and the South Pacific at 160°W for both DJF and JJA. However, contrasting negative trends in the equatorial central Pacific for DJF may be related to ENSO although these trends are not statistically significant. Trends in CWV_cc (Figures 9b and 10b), which are the expected trends determined by thermodynamic response to changes in near surface temperature, are generally not significant over the ocean. The CWV trends are primarily explained by the dynamical contribution, CWV_dyn (Figures 9c and 10c). However, significant positive trends in the north and northwest Pacific for DJF are enhanced by thermodynamic increases in water vapor in response to ocean warming. This appears consistent with Trenberth *et al.* [2005] who analyzed the period 1988–2004 for SSM/I data. However,

here we suggest that changes in dynamics associated with the changes in surface temperature act to enhance the CWV trends associated directly with the warming.

[29] Over land regions, significant trends in CWV are generally negative over the period 1979–2001, in particular for equatorial Africa and Brazil. Over these regions, the significant trends in CWV_cc are positive, relating to increases in near surface temperature in ERA40 over these regions. Therefore the changes in water vapor are of opposite sign to that expected from a thermodynamic response to changes in temperature. One possible explanation for this is that clouds and humidity reduced during the period, allowing greater solar radiation to heat the surface directly. Without the available water supply over land regions, the CWV is not so strongly influenced by the thermodynamic relationship between water vapor and temperature observed over the ocean. Moreover, where surface water availability is low it is likely that increases in temperature will result in reduced RH because there is not enough water available to allow specific humidity to increase in line with the Clausius-Clapeyron equation. To investigate this possibility further and to investigate the relationships between CWV and precipitation, we now

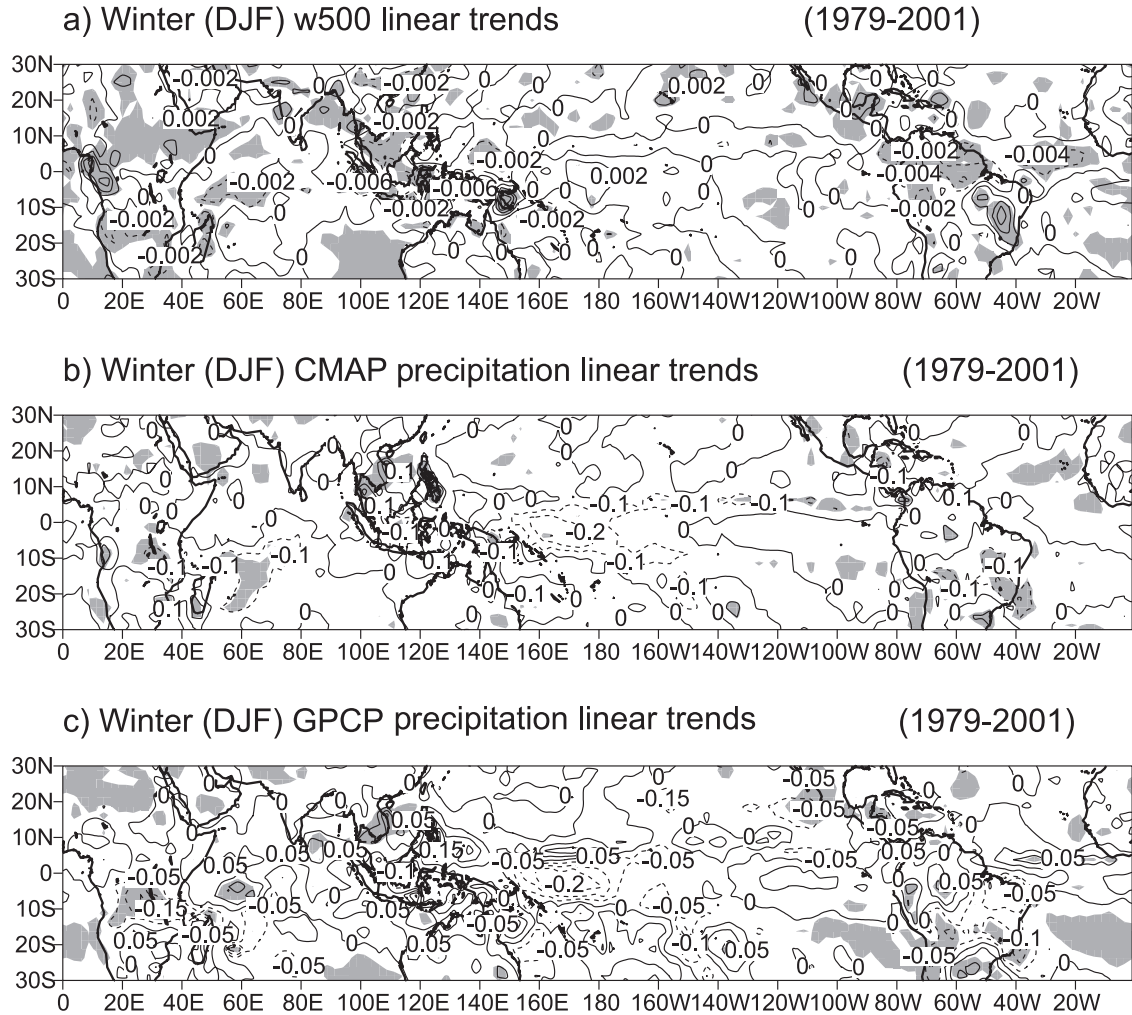


Figure 11. Linear trends of (a) 500 hPa vertical motion (hPa/s) from ERA40, (b) precipitation from CMAP (mm), and (c) precipitation from GPCP (mm) for DJF, 1979–2001. Dashed curves depict negative trends, and shaded areas indicate 95% significance level.

present linear trends in precipitation and vertical motion for DJF (Figure 11) and JJA (Figure 12).

[30] The changes in ERA40 500 hPa vertical motion (ω_{500}) are presented in Figures 11a and 12a. Note that increases in ω_{500} (solid contours) denote a decrease in upward motion while negative trends in ω_{500} (dashed contours) indicate increased upward motion. Again, shaded regions denote trends that are significant at the 95% confidence level. It is first apparent that the spatial maps of ω_{500} trends are highly heterogeneous. We also analyzed NCEP vertical motion fields (not shown); these were found to be less noisy than ERA40 but display many of the same statistically significant trends. Also it is not clear that the nature of the ERA40 ω_{500} field is unrealistic; *Trenberth and Guillemot* [1998] suggested that the divergent circulation in the NCEP/NCAR reanalysis was too weak.

[31] Trends in precipitation are also calculated for the CMAP and GPCP data sets in Figures 11 and 12. These display large differences over the ocean. *Yin et al.* [2004] note that oceanic trends in CMAP data may be erroneous because of questionable use of atoll data for calibration.

However, over land the two data sets are in closer agreement.

[32] Comparing Figures 9–12, correspondence between the spatial maps of trends in water vapor, vertical motion and precipitation appears weak. However, significant negative trends in ω_{500} over the equatorial Atlantic for DJF and JJA, denoting increased ascent and convective activity, are consistent with positive trends in CWV. These trends in CWV and ω_{500} are not accompanied by significant trends in precipitation. Decreasing trends in CMAP precipitation are thought to be an artefact of input data and problems with the use of atoll data in the merged product [*Yin et al.*, 2004].

[33] There is a slight, but significant, negative trend in GPCP precipitation to the west of the Australian, South American and Namibian marine stratocumulus regions during DJF (Figure 11c). This is accompanied by significant positive trends in ω_{500} (more stable conditions). An increasing trend in CWV is particularly significant over the southeast Pacific, which is determined mainly by the dynamical component (CWV_{dyn}; Figure 9c) but offset by a slight reduction in the thermodynamic contribution

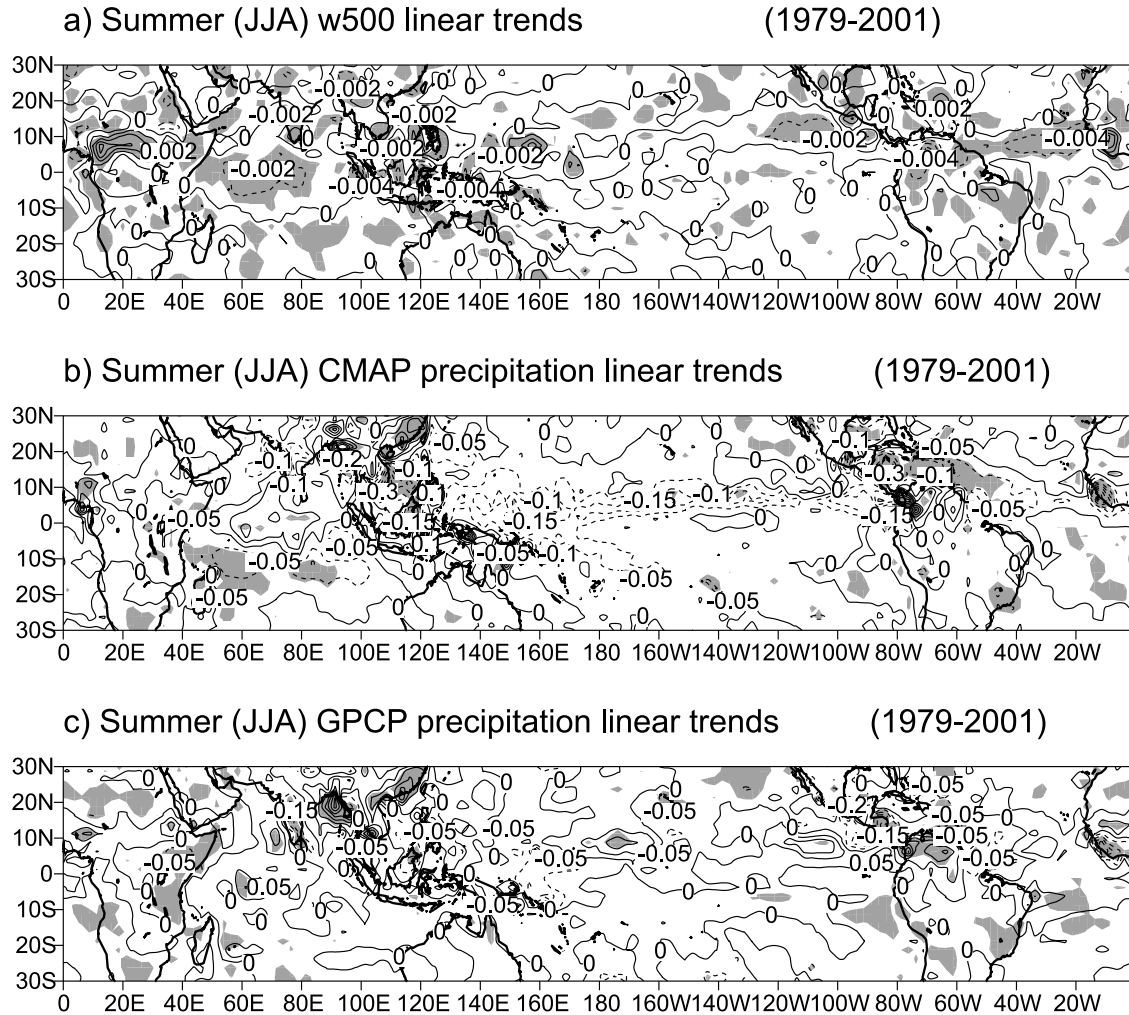


Figure 12. As Figure 11 but for JJA, 1979–2001.

(CWV_cc; Figure 9b). This is suggestive of enhanced water vapor but reduced precipitation and convective activity associated with an ocean cooling over this region.

[34] Over the North Pacific, dynamic and thermodynamic contributions to increased CWV do not appear to coincide with coherent trends in vertical motion or precipitation. The reduction in CWV over equatorial Africa and Brazil is associated with significant positive trends in ω_{500} (less ascending motion) but trends in precipitation are not significant. The consistency between reduced CWV and reduced ascent over land supports the hypothesis that reduced cloud and humidity may allow greater heating of the surface, as indicated by the positive trend in CWV_cc. It is possible that changes in the character of precipitation [e.g., Trenberth *et al.*, 2003] allow a reduction of convective activity while maintaining constant precipitation. However, the uncertainty associated with the ERA40 and GPCP data and the relatively low temporal resolution considered preclude the identification of such mechanisms in the present study.

4.2. Analysis of Regional Time Series

[35] To analyze specific features in regional variability of CWV and its links to precipitation, we constructed time

series of regionally averaged anomalies of the seasonal mean CWV, CWV_cc, CWV_dyn and CMAP precipitation for the period of 1979–2001. The regions have been selected based, mainly, on the criteria of large local variability of CWV revealed from analyses of standard deviations (Figures 4 and 5) and leading EOF modes (Figures 6 and 7). These regions include Africa (10° – 0° N, 25° – 35° E), India (25° – 15° N, 72.5° – 82.5° E), western Pacific (15° – 5° N, 125° – 135° E), Maritime Continent (0° – 10° S, 110° – 120° E), Australia (15° – 25° S, 125° – 135° E), central equatorial Pacific (2.5° N to 7.5° S, 150° – 140° W), eastern equatorial Pacific (2.5° N to 7.5° S, 90° – 80° W), and Brazil (7.5° – 17.5° S, 52.5° – 42.5° W). In each region, data from 25 grid points were used to estimate regional averages. Time series of normalized anomalies of seasonal mean CWV and precipitation for each of these regions are shown in Figures 13 and 14. To aid comparison, each time series is normalized by its standard deviation. Correlation coefficients between CWV, CWV_cc, CWV_dyn and CMAP precipitation in each of the above regions are presented in Table 1. Coefficients that are statistically significant at the 95% confidence level according to Student's *t*-test [Bendat and Piersol, 1966] are presented in bold.

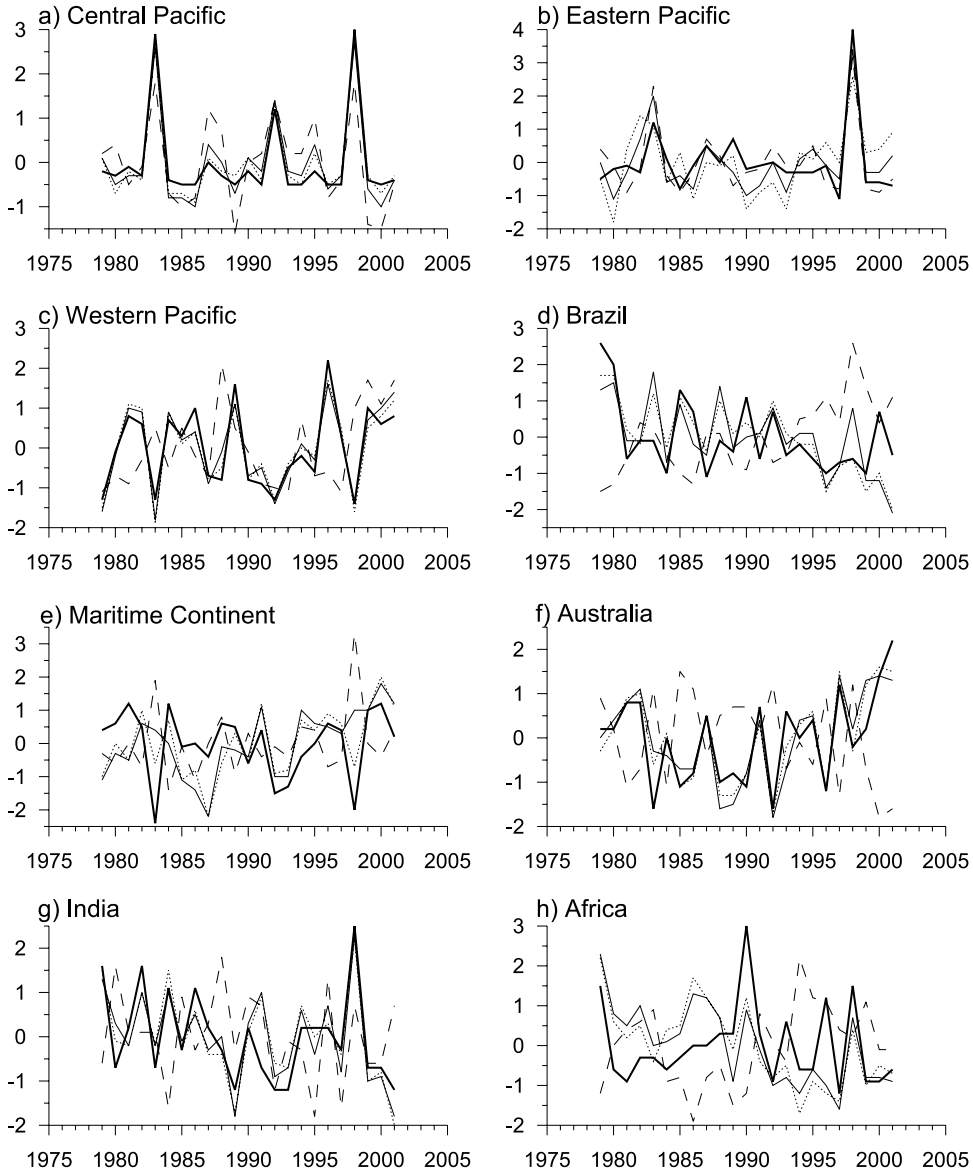


Figure 13. Time series of normalized anomalies of CMAP precipitation (red curve), CWV (blue curve), CWV_cc (green curve), and CWV_dyn (brown curve) for DJF, 1979–2001. See color version of this figure in the HTML.

[36] As seen in Figures 13a and 14a and Table 1, over the central Pacific all three parameters (i.e., CWV, CWV_cc and CWV_dyn) are strongly linked to variability of precipitation both during winter and summer seasons (here and further in the text we mean boreal winter and summer seasons). Note, however, that during winter, the relative role of the dynamic component in regional precipitation variability is larger (respective correlation is 0.98) than that of the thermodynamic component. All parameters show significant maximums associated with the largest (during considered period) ENSO events of 1982/3 and 1997/8.

[37] In contrast to the central Pacific, CWV_cc is a major factor that defines precipitation variability over the eastern Pacific both in winter and summer (see Figures 13b and 14b and Table 1). It is interesting to note that during summer the dynamic component of CWV reduces significantly the

regional relationship between CWV and precipitation. In particular, it is clearly seen that during ENSO events CWV_dyn is almost out of phase with other parameters (Figure 14b).

[38] Over the western Pacific, CWV_dyn appears to completely determine regional precipitation variability during winter (Figures 13c and 14c) and there is very strong correlation (0.94) between respective time series. During summer CWV is not linked with precipitation (correlation is 0.15). Though both CWV_cc and CWV_dyn show significant correlations (-0.65 and 0.42, respectively) with precipitation, they cancel the effects of each other resulting in very low correlation between CWV and precipitation. It is worth noting that consistent with the EOF analysis, variations over the western Pacific are out of phase with those over the central Pacific (Figures 13a and 13c).

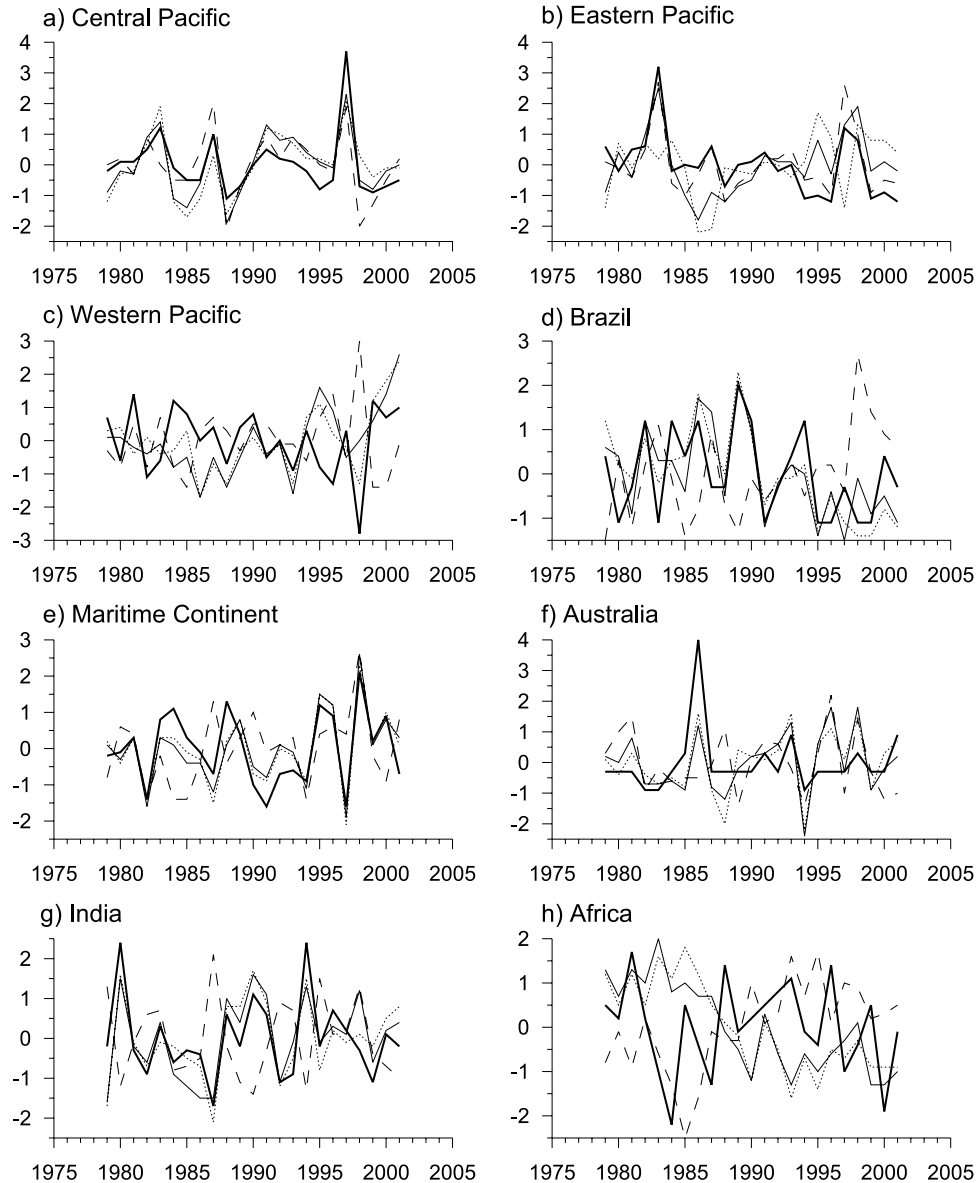


Figure 14. As Figure 13 but for JJA, 1979–2001. See color version of this figure in the HTML.

[39] As seen in Figures 13d and 14d and Table 1, over Brazil CWV_{dyn} is a major factor in determining the correspondence between CWV and precipitation both during winter and summer seasons (respective correlations are 0.70 and 0.75). However, CWV_{cc} significantly counteracts the effect of the dynamical component. In general, like in the case of the central Pacific, there is no seasonality in relations between CWV and precipitation over Brazil.

[40] Over the Maritime Continent (Figures 13e and 14e and Table 1), there is no link between CWV and regional precipitation variability during winter. Though both CWV_{cc} and CWV_{dyn} show significant correlations (−0.66 and 0.52, respectively) with precipitation, they cancel the effects of each other resulting in very low correlation between CWV and precipitation (0.18). On the contrary, during summer season CWV is strongly linked to regional precipitation (correlation is 0.84); the dynamic component is the major factor determining this link.

[41] During boreal winter (Australian monsoon season) over Australia, all three parameters (i.e., CWV, CWV_{cc} and CWV_{dyn}) are strongly linked to variability of regional precipitation (Figure 13f and Table 1). Note that the large negative correlation (−0.86) between CWV_{cc} and precipitation does not reduce significantly the dominating relationship between the dynamic component and precipitation. This is because magnitudes of CWV_{cc} variability in this region are significantly lower than those of CWV_{dyn} (Figure 4). During summer (Figure 14f) the leading role of CWV_{dyn} in variability of precipitation over northern Australia is evident (correlation is 0.55).

[42] Over India (Figures 13g and 14g and Table 1), the dynamic component is a major contributor to interannual variability of precipitation both during winter and summer seasons (respective correlations are 0.86 and 0.80). Significant negative correlation (−0.57) between CWV_{cc} and

Table 1. Correlation Coefficients Between Regional Time Series of CWV, CWV_cc, and CWV_dyn and CMAP and GPCP Precipitation Estimated for DJF and JJA^a

	DJF Precipitation	JJA Precipitation
<i>Central Pacific</i>		
CWV	0.95 (0.94)	0.80 (0.81)
CWV_cc	0.71 (0.71)	0.72 (0.65)
CWV_dyn	0.98 (0.97)	0.71 (0.76)
<i>Eastern Pacific</i>		
CWV	0.80 (0.82)	0.54 (0.72)
CWV_cc	0.84 (0.83)	0.84 (0.93)
CWV_dyn	0.52 (0.54)	-0.31 (-0.17)
<i>Western Pacific</i>		
CWV	0.93 (0.93)	0.15 (0.12)
CWV_cc	0.13 (0.15)	-0.65 (-0.54)
CWV_dyn	0.94 (0.94)	0.42 (0.36)
<i>Brazil</i>		
CWV	0.54 (0.48)	0.64 (0.66)
CWV_cc	-0.65 (-0.57)	-0.48 (-0.48)
CWV_dyn	0.70 (0.62)	0.75 (0.77)
<i>Maritime Continent</i>		
CWV	0.18 (0.16)	0.84 (0.83)
CWV_cc	-0.66 (-0.70)	0.16 (0.15)
CWV_dyn	0.52 (0.52)	0.87 (0.87)
<i>Australia</i>		
CWV	0.83 (0.83)	0.45 (0.59)
CWV_cc	-0.86 (-0.85)	-0.05 (0.11)
CWV_dyn	0.90 (0.90)	0.55 (0.64)
<i>India</i>		
CWV	0.83 (0.77)	0.75 (0.69)
CWV_cc	-0.05 (-0.14)	-0.57 (-0.55)
CWV_dyn	0.86 (0.82)	0.80 (0.75)
<i>Africa</i>		
CWV	0.45 (0.50)	-0.07 (-0.01)
CWV_cc	-0.35 (-0.40)	0.02 (0.01)
CWV_dyn	0.47 (0.53)	-0.07 (-0.01)

^aCorrelation coefficients with GPCP precipitation are given in parentheses. Coefficients that are significant at the 95% confidence levels are presented in bold.

precipitation during summer only slightly reduces the influence of the dynamic component.

[43] During winter CWV_dyn is significantly correlated (0.47) with precipitation over Africa (Figure 13h and Table 1). The relationship between CWV_dyn and precipitation variability is slightly counteracted by the thermodynamic component. None of the considered parameters is associated with regional precipitation variability during summer. Thus, during boreal summer, precipitation variability over Africa is not influenced by variations of CWV.

[44] Though there are some minor differences, correlations with GPCP precipitation are generally consistent with above considered correlations with CMAP precipitation. In general, these differences rarely exceed 0.1 (Table 1). This suggests relatively good agreement between the two precipitation data sets on interannual timescale.

[45] Analysis of the regional time series performed in this section has shown that in the tropics there are regions where seasonal differences in interannual behavior of CWV are very small (e.g., central Pacific). However, there are also

regions where interannual variability of CWV is clearly season dependent (e.g., Australia). In general, in many regions seasonality is also well pronounced in relationships between CWV and precipitation. It is shown that in different regions/seasons dynamic and thermodynamic components of CWV play different roles in variability of precipitation. In some regions (e.g., Brazil, central Pacific) seasonality in relationships between CWV and precipitation was not detected.

5. Conclusions

[46] Analysis of water vapor variability and its links with dynamics and precipitation were conducted over the period 1979–2001 using the ERA40 reanalysis and additional data sets. Using vertical motion and near-surface temperature fields, the spatial and temporal signal of column-integrated water vapor (CWV) variability are partitioned between dynamic and thermodynamic contributions. The main conclusions of the present study are as follows:

[47] 1. The spatial distribution of water vapor is explained primarily by the thermodynamic relationship between water vapor and temperature, assuming a near-constant relative humidity.

[48] 2. The large-scale atmospheric circulation acts to increase the CWV locally over regions of low-level convergence. These regions are primarily the south Indian Ocean, the tropical west and South Pacific and Brazil for DJF. For JJA, the Africa and Indian monsoon region CWV is increased because of the dynamic contribution; this effect also influences the ITCZ and tropical western Pacific regions to a lesser extent.

[49] 3. The equatorial central Pacific at 160°W is affected by a negative contribution to CWV due to the local dynamics. This situation reverses during El Niño events, when moisture convergence influences the region.

[50] 4. The temporal variability of CWV is strongly dominated by the dynamic component of CWV variations. Only the central and eastern equatorial Pacific is noticeably influenced by thermodynamic variations in CWV. Here the dynamics and thermodynamics both contribute to CWV variations.

[51] 5. Temporal variability in CWV is dominated by ENSO, in particular the 1982/3 and 1997/8 El Niño events. The 1986–1989 ENSO cycle is influenced by the dynamic and thermodynamic variability of CWV while the early 1990s El Niño is influenced more by the dynamic influence rather than thermodynamics. This highlights the differing nature of individual ENSO events.

[52] 6. Significant trends in CWV over the ocean are primarily positive. Significant negative trends in CWV are identified over equatorial Africa and Brazil. The dynamical component of CWV dominates the trends. This is particularly evident over equatorial Africa and Brazil where the negative CWV trends are of opposite sign to that expected from the positive trends in CWV_cc relating to increasing temperatures. Over land, changes in cloud cover, associated with reduced convective activity diagnosed from increasing ω_{500} may explain the warming trend. Without the availability of surface water, the warming trend is not associated with the increased CWV expected from the Clausius-Clapeyron equation.

[53] 7. Trends in precipitation lack coherence, and there appears little association with trends in CWV. The negative trends in CMAP precipitation over the ocean are thought to be spurious [Yin *et al.*, 2004]. However, negative trends in GPCP precipitation over marine stratocumulus regions in the Southern Hemisphere summer are associated with increased water vapor, reduced ascending motion and slight ocean cooling, most noticeably in the southeast Pacific. Over this region, reduced ascent is usually associated with increased boundary layer humidity and associated stratocumulus [Klein, 1997], which act to cool the surface during the daytime. These trends may be influenced by the changes in stratocumulus during ENSO evolution.

[54] 8. Over many tropical regions interannual variability of precipitation is strongly linked to CWV variations during both winter and summer seasons. However, over some regions (western Pacific, Maritime Continent, Africa) such links are observed only during one of two considered seasons. Although the dynamic component of CWV is a major agent for precipitation variability, in some regions/seasons the thermodynamic component cancels its effect on precipitation variability.

[55] Diagnosing the links between CWV and precipitation is complex. Changes in SST can impact the large-scale atmospheric circulation, which in turn contributes to dynamical changes in water vapor and precipitation. Additionally, thermodynamics will also cause local changes in SST to impact the CWV. Over land, the lack of water supply changes the nature of the surface temperature dependence of CWV. There is some evidence for increasing trends in CWV due to thermodynamics alone, mainly over the north and northwest Pacific. However, even in these regions, the direct response of CWV to changes in temperature appears to be enhanced by dynamical changes.

[56] Over the period 1979–2001, changes in the large-scale circulation, primarily associated with ENSO teleconnections, dominate the variability and trends in CWV compared to the smaller thermodynamic response of water vapor to changes in temperature. Links between precipitation and water vapor are not clear on the decadal timescale; this may partly reflect the inadequacies in the precipitation data sets and reanalysis products over such long timescales.

[57] **Acknowledgments.** This research was supported by Russian Foundation for Basic Research grant 02-05-64498. R. P. Allan was supported by NERC grant NE/C51785X/1. The manuscript was improved by the constructive comments of the two anonymous reviewers. The ERA40 data were retrieved from the ECMWF data services, the SMMR data were retrieved from the NASA Langley DAAC, the SSM/I data were retrieved from <http://www.ssmi.com>, the GPCP data were retrieved from <http://www.ncdc.noaa.gov>, and the CMAP data were retrieved from <ftp://ftpprd.ncep.noaa.gov>.

References

- Adler, R. F., *et al.* (2003), The Version-2 Global Precipitation Climatology Project (GPCP) monthly precipitation analysis (1979–present), *J. Hydrometeorol.*, **4**, 1147–1167.
- Allan, R. P., M. A. Ringer, J. A. Pannett, and A. Slingo (2004), Simulation of the Earth's radiation budget by the European Centre for Medium Range Weather Forecasts 40-year Reanalysis (ERA40), *J. Geophys. Res.*, **109**, D18107, doi:10.1029/2004JD004816.
- Bendat, J. S., and A. G. Piersol (1966), *Measurement and Analysis of Random Data*, 390 pp., John Wiley, Hoboken, N. J.
- Bony, S., J.-L. Dufresne, H. Le Treut, J. J. Morcrette, and C. A. Senior (2004), On dynamical and thermodynamical components of cloud changes, *Clim. Dyn.*, **22**, 71–86.
- Bretherton, C. S., M. E. Peters, and L. E. Back (2004), Relationships between water vapor path and precipitation over the tropical oceans, *J. Clim.*, **17**, 1517–1528.
- Diaz, H. F., M. P. Hoerling, and J. K. Eischeid (2001), ENSO variability, teleconnections and climate change, *Int. J. Climatol.*, **21**, 1845–1862.
- Gershunov, A., and R. Roca (2004), Coupling of latent heat flux and the greenhouse effect by large-scale tropical/subtropical dynamics diagnosed in a set of observations and model simulations, *Clim. Dyn.*, **22**, 205–222.
- Huffman, G. J., *et al.* (1997), The Global Precipitation Climatology Project (GPCP) combined precipitation dataset, *Bull. Am. Meteorol. Soc.*, **78**, 5–20.
- Intergovernmental Panel on Climate Change (IPCC) (2001), *Climate Change 2001: The Scientific Basis*, 944 pp., Cambridge Univ. Press, New York.
- Klein, S. A. (1997), Synoptic variability of low-cloud properties and meteorological parameters in the subtropical trade wind boundary layer, *J. Clim.*, **10**, 2018–2036.
- Luo, Z., and W. B. Rossow (2004), Characterizing tropical cirrus life cycle, evolution, and interaction with upper tropospheric water vapor using lagrangian trajectory analysis of satellite observations, *J. Clim.*, **17**, 4541–4563.
- North, G. R., T. L. Bell, and R. F. Calahan (1982), Sampling errors in the estimation of empirical orthogonal functions, *Mon. Weather Rev.*, **110**, 699–706.
- Raval, A., and V. Ramanathan (1989), Observational determination of the greenhouse effect, *Nature*, **342**, 758–761.
- Soden, B. J. (2004), The impact of tropical convection and cirrus on upper tropospheric humidity: A Lagrangian analysis of satellite measurements, *Geophys. Res. Lett.*, **31**, L20104, doi:10.1029/2004GL020980.
- Sohn, B.-J., and J. Schmetz (2004), Water vapor-induced OLR variations associated with high cloud changes over the tropics: A study from Meteosat-5 observations, *J. Clim.*, **17**, 1987–1996.
- Sohn, B.-J., E. A. Smith, F. R. Robertson, and S.-C. Park (2004), Derived over-ocean water vapour transports from satellite-retrieved E-P datasets, *J. Clim.*, **17**, 1352–1365.
- Spencer, H. (2004), Role of the atmosphere in seasonal phase locking of El Niño, *Geophys. Res. Lett.*, **31**, L24104, doi:10.1029/2004GL021619.
- Trenberth, K. E., and C. J. Guillemot (1998), Evaluation of the atmospheric moisture and hydrological cycle in the NCEP/NCAR reanalyses, *Clim. Dyn.*, **14**, 213–231.
- Trenberth, K. E., A. Dai, R. M. Rasmusson, and D. B. Parsons (2003), The changing nature of precipitation, *Bull. Am. Meteorol. Soc.*, **84**, 1205–1217.
- Trenberth, K. E., J. Fasullo, and L. Smith (2005), Trends and variability in column-integrated atmospheric water vapor, *Climate Dyn.*, **24**, 741–758.
- Uppala, S. M., *et al.* (2005), The ERA-40 Re-analysis, *Q. J. R. Meteorol. Soc.*, in press.
- von Storch, H., and A. Navarra (1995), *Analysis of Climate Variability*, 334 pp., Springer, New York.
- Wentz, F. J. (1997), A well-calibrated ocean algorithm for SSM/I, *J. Geophys. Res.*, **102**, 8703–8718.
- Wentz, F. J., and E. A. Francis (1992), Nimbus-7 SMMR ocean products 1979–1984, *Tech. Rep. 033192*, Remote Sens. Syst., Santa Rosa, Calif.
- Wilks, D. S. (1995), *Statistical Methods in the Atmospheric Sciences*, 467 pp., Elsevier, New York.
- Xie, P., and P. Arkin (1996), Analyses of global monthly precipitation using gauge observations, satellite estimates, and numerical model predictions, *J. Clim.*, **9**, 840–858.
- Xie, P., and P. Arkin (1997), Global precipitation: A 17-year monthly analysis based on gauge observations, satellite estimates, and numerical model outputs, *Bull. Am. Meteorol. Soc.*, **78**, 2539–2558.
- Yin, X., A. Gruber, and P. Arkin (2004), Comparison of the GPCP and CMAP merged gauge-satellite monthly precipitation products for the period 1979–2001, *J. Hydrometeorol.*, **5**, 1207–1222.
- Zvereva, I. I., and P. Chu (2003), Recent climate changes in precipitable water in the global tropics as revealed in National Centers for Environmental Prediction/National Center for Atmospheric Research reanalysis, *J. Geophys. Res.*, **108**(D10), 4311, doi:10.1029/2002JD002476.
- R. P. Allan, Environmental Systems Science Centre, University of Reading, Harry Pitt Building, 3 Earley Gate, Whiteknights, Reading RG6 6AL, UK.
- I. I. Zvereva, P. P. Shirshov Institute of Oceanology, RAS, 36 Nakhimovsky Avenue, Moscow 117997, Russia. (igor@saif.msk.ru)